Peer-reviewed version available at Colloids Interfaces 2018, 2, 56; doi:10.3390/colloids2040056

Review

Sessile Droplets on Deformable Substrates

Gulraiz Ahmed [1,2], Nektaria Koursari [1], Anna Trybala [1] and Victor M. Starov [1,*]

[1] Department of Chemical Engineering, Loughborough University, Loughborough, Leicestershire LE11 3TU, United Kingdom;
[2] Department of Mechanical Engineering, University of Central Punjab, Lahore, Pakistan; gulraiz.ahmed@ucp.edu.pk
* Correspondence: v.m.starov@lboro.ac.uk; Tel.: +44(0)1509 222508

Abstract: Wetting of deformable substrates has gained significant interest over the past decade due to its extensive applications and uses. This interest has developed due to technological advances which are able to capture interfacial behavior taking place when a liquid droplet is placed on a deformable substrate. Researchers have developed different theories to explain processes taking place in the process of wetting of deformable/soft substrates. For the scope of this review, we will consider the fluid to be Newtonian, partially wetting, and surface forces are incorporated with the help of disjoining/conjoining pressure acting in the vicinity of the apparent, three-phase contact line. The following subjects are briefly reviewed: (i) Equilibrium of droplets on soft substrates. It is shown that properties of the disjoining/conjoining pressure isotherm and properties of the deformable substrate determine both the shape of the liquid droplet and deformation of the substrate; (ii) Equilibrium conditions of droplets on deformable substrates. It is shown that for a droplet to be at equilibrium on a deformable substrate under consideration, Jacobi's sufficient condition is satisfied; (iii) Hysteresis of contact angle of sessile droplets on deformable substrates. It is shown that as the elasticity of the deformable substrate is increased, both advancing and receding contact angles are reduced.

Keywords: deformable substrates; surface forces; droplets; hysteresis

1. Introduction

Wetting of deformable substrates has gained significant interest over the last decades. Particularly due to its wide range of applications. These applications occur both naturally (include biological processes) and via industrial processes. For instance inkjet printing applications [1], forensics [2], surface coating, pesticide spraying, spray painting [3], etc.

Young's equation is well-known and has been widely used to predict equilibrium contact angle, θ_e, on solid/rigid substrates [4]. It gives a relationship between solid-liquid, liquid-vapor, and vapor-solid surface tensions and based on consideration of balance of horizontal forces. When the substrate is deformable the Young's equation cannot be used, because it ignores vertical force balance. An extra term for the vertical force balance ($\gamma \sin \theta_e$) appears, which remains unbalanced. Substrate deformation must balance this extra force in the case of deformable substrate. However even after modification Young's equation cannot be applied directly as it gives rise to deformation singularity (surface deformation goes to infinity) near the three-phase contact line [5–10]. To avoid this singularity researchers have tried different approaches. Initially it was suggested that surface tension should be uniformly distributed near the contact line to mitigate the singularity [6–10]. Another approach is to consider surface forces acting in thin precursor film on the substrate, where the contact line is replaced with a smooth transition from the bulk of the liquid to the thin film. This inclusion of thin film removes deformation singularity. Disjoining/conjoining pressure is used to consider this smooth transition inside the apparent three-phase contact line. It describes the action of surface forces near the apparent three-phase contact line [11]. Disjoining/conjoining pressure approach was first introduced by Derjaguin for droplets on solid substrates [12]. More recently it was shown that this approach can also be used for droplets on deformable substrates [11,13–17].

Recently, experimental studies on droplet wetting of deformable substrate have gained a lot of interest primarily due to technological advances in imaging techniques [18–22]. In the past few years it has been possible to record high resolution images both in temporal and spatial coordinates. These high-resolution cameras allow capturing droplet profiles in the vicinity of the three-phase contact line and subsequent substrate deformations. This has allowed building understanding of theoretical concepts underlying in experiments [23–26]. Recent progress of theoretical studies for the equilibrium and hysteresis of contact angles of sessile droplets under the influence of disjoining/conjoining pressure were developed [14,16,17] and reviewed below.

In the next section, a new modeling technique for the investigation of wetting of soft substrates is reviewed, where a three-dimensional liquid droplet on a soft substrate is considered. Surface forces are introduced using simplified disjoining/conjoining pressure isotherm. Elasticity of the soft substrate is introduced using Winkler's model [27]. Substrate's deformation is directly dependent upon the physical characteristics of the disjoining/conjoining pressure isotherm and substrate's physical properties [14].

For the droplet to be at equilibrium, four conditions have to be satisfied: (i) first variation of excess free energy is equal to zero; (ii) second variation is greater than zero; (iii) transversality condition is satisfied; (iv) Jacobi's sufficient condition is fulfilled. Fourth condition is usually forgotten by researchers in this area. Recently there was a successful attempt to fulfill the essential fourth condition for the liquid droplet on a soft substrate [16]. In section 3 the verification of the Jacobi's sufficient condition for already obtained solution of equilibrium droplets on deformable substrates is undertaken.

Contact angle hysteresis (advancing and receding contact angles) is broadly thought to exist due to surface roughness and local surface heterogeneities. These are not the only causes for the existence of contact angles hysteresis. Lately researchers have illustrated that hysteresis exist on smooth homogeneous solid substrates, which are chemically homogeneous as well [28–30]. Recently this knowledge was extended to introduce the theory of contact angle hysteresis on smooth deformable substrates [17]. In section 4, the findings of these quasi-equilibrium states that exist on deformable substrates is discussed.

2. Equilibrium of droplets on soft substrates

In this section a new approach for wetting of soft substrates is developed by introducing, surface forces action in the vicinity of three-phase contact line. A simplified linear disjoining/conjoining pressure isotherm, Π, and elasticity of the substrate through Winkler's model [27,31] are used in this section. According to the Winkler's model, the deformation in the soft substrate is regional and has a direct relation with the applied pressure, P [14]:

$$h_s = -KP, \tag{1}$$

where, K is the elasticity coefficient, h_s is the local deformation of the substrate due to the applied pressure from the fluid above, see Figure 1.

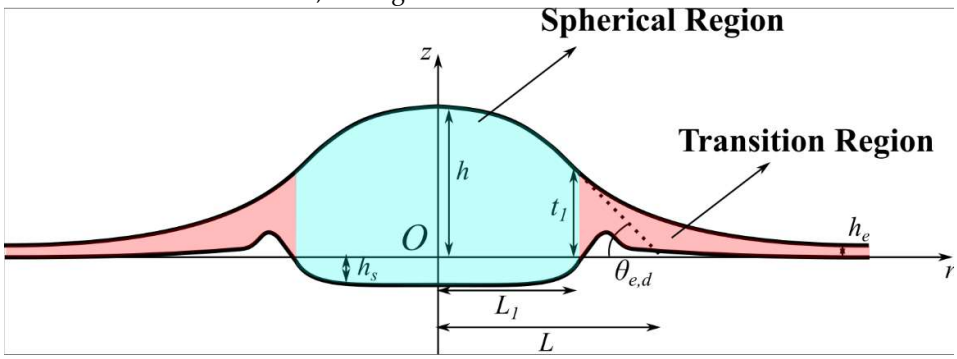

Figure 1: Schematic diagram of droplet on a deformable substrate, Spherical (Bulk) region - $\Pi(h - h_s) = 0$, and Transition region - $\Pi(h - h_s) \neq 0$, h - the liquid profile; h_s - deformation of the substrate; h_e- equilibrium flat film; θ_e- apparent equilibrium contact angle; t_1- height of the droplet

at which surface forces (disjoining/conjoining pressure) start to act; L_1- radial length corresponding to t_1; L- Effective radius of the droplet; r, $z-$ co-ordinate system.

Assume P_{air} to be the ambient pressure in the air. Under the influence of the ambient air pressure the soft solid deformation is given by:

$$h_{se} = -KP_{air}. \tag{2}$$

Equilibrium thin film of fluid covers the deformed soft substrate, which is calculated according to a combination of the Kelvin's equation and disjoining/conjoining pressure isotherm [11]:

$$\Pi(h_e) = P_e = \frac{R_g T}{v_m} \ln \frac{p_{sat}}{p}, \tag{3}$$

where, v_m is the molar volume of the liquid, T is the temperature in K, R_g is the gas constant, vapor pressure, p, which is higher than the saturated pressure p_{sat}. Reminder, a droplet is deemed to be at equilibrium under oversaturated vapor only according to Kelvin's equation. The excess free energy of the equilibrium thin film on the deformed solid in front of the liquid droplet per unit area is given by [11,14]:

$$\frac{F_{e,film}}{S_{film}} = \gamma + \gamma_s + P_e h_e + \frac{h_{se}^2}{2K} + \int_{h_e}^{\infty} \Pi(h) dh, \tag{4}$$

where, $P_e = P_{air} - P_{liquid}$, γ and γ_s are vapor-liquid and liquid-solid surface tensions. This free energy should be subtracted from the free energy of the droplet on the deformable substrate; otherwise the excess free energy of the droplet is infinite [11,14]. Hence, the excess free energy of the droplet on a deformable solid substrate is as follows (see Figure 1):

$$F - F_{e,film} = \gamma \Delta S + \gamma_s \Delta S_s + \Delta V + F_{surface\ forces} + F_{deformation}, \tag{5}$$

where Δ means "as compared with a flat equilibrium film".
Eq. (5) can be rewritten as:

$$F - F_{e,film} = 2\pi \int_0^{\infty} f(h, h', h_s, h_s') dr, \tag{6}$$

where

$$f(h, h', h_s, h_s') = r \left[\begin{array}{c} \gamma\sqrt{1 + h'^2(r)} - \gamma + \gamma_s\sqrt{1 + h_s'^2(r)} - \gamma_s + \\ P_e(h - h_s) - P_e h_e + \frac{h_s^2}{2K} - \frac{h_{se}^2}{2K} \\ + \int_{h-h_s}^{\infty} \Pi(h) dh - \int_{h_e}^{\infty} \Pi(h) dh \end{array} \right]. \tag{7}$$

In above equations, r is the length along radial direction. For equilibrium conditions, the excess free energy in Eq. (6) should attain minimum value. To fulfil this condition the first variation Eq. (6) should equal to zero, which leads to two Euler equations, i.e. for liquid and substrate profiles:

$$\frac{\gamma}{r} \frac{d}{dr} \frac{rh'}{(1 + h'^2)^{1/2}} + \Pi(h - h_s) = P_e, \tag{8}$$

$$\frac{\gamma_s}{r} \frac{d}{dr} \frac{rh_s'}{(1 + h_s'^2)^{1/2}} - \Pi(h - h_s) - \frac{h_s}{K} = -P_e. \tag{9}$$

Eqs. (8) and (9) form a system of two interlinked differential equations for two undetermined profiles: the fluid droplet, $h(r)$, and deformed soft substrate, $h_s(r)$. Low slope approximation, $h'^2 \ll 1$, $h_s'^2 \ll 1$, which is acceptable for small contact angles, is used below. It is important to observe that Eq. (8) is unlike the usual capillary equation for the non-deformable substrate, because it now has contribution of h_s in the disjoining/conjoining pressure, which can be determined using Eq. (9). Eqs. (8) and (9) are interconnected and, in general can be solved numerically only. It is the reason why the problem is further simplified with use of linear disjoining/conjoining pressure isotherm to obtain analytical solutions.

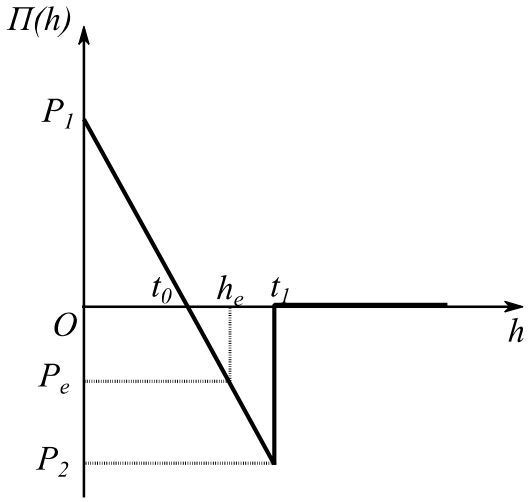

Figure 2: Disjoining/conjoining pressure isotherm adopted for calculations. Reproduced with permission from Ref. [14]. Copyright © 2017 Elsevier B.V.

$$\Pi(h) = \begin{cases} P_1 - ah & at \;\; h \le t_1 \\ 0 & at \;\; h > t_1 \end{cases}. \qquad (10)$$

where P_1 and t_0 are defined in Figure 2, t_1 is the radius of influence of surface forces, a is the slope of disjoining/conjoining pressure isotherm. The subsequent radial length from the origin to the point t_1 is L_1, see Figure 1. The selected linear dependency of disjoining/conjoining pressure isotherm $\Pi(h)$ on h according to Eq. (10) still portrays the essential properties of the disjoining/conjoining pressure isotherm in spite of substantial simplification: (i) it satisfies the stability condition, $\Pi'(h) < 0$ when $h < t_1$; (ii) the influence of surface forces is short ranged and the radius of its action is defined by t_1; (iii) it corresponds to the partial wetting case at the proper choice of parameters [14].

Disjoining/conjoining pressure cannot be ignored near the apparent three-phase contact line; therefore, substrate deformation is linked directly with the parameters of the disjoining/conjoining pressure isotherm, see Table 1.

Table 1: Physical properties used for calculation of droplet profile and deformation in the substrate [14].

Physical Property	Value
γ	72 dyne/cm
t_1	3×10^{-6}cm
t_0	7×10^{-7} cm
a	1×10^{11} dyne/cm^3
K	1×10^{-11} cm^3/dyne
P_e	-1×10^{5} dyne/cm^2
γ_s	1 dyne/cm

Effect of variation of P_e, a, K and γ_s on substrate deformation and its subsequent effect on the droplet profile is investigated below.

2.1. Effect of variation of excess pressure, P_e

Excess pressure is changed according to $0 \le |P_e| \le |P_2|$. Figure 3 illustrate shapes of the droplet and substrate with variation in P_e. An increase in P_e causes equilibrium thin film height, h_e, to reduce. This consequently influences the height and span of the droplet to increase. Hence, causing the extent of the deformation in the radial direction to grow, but generates a reduction in the depth which the substrate gets deformed to.

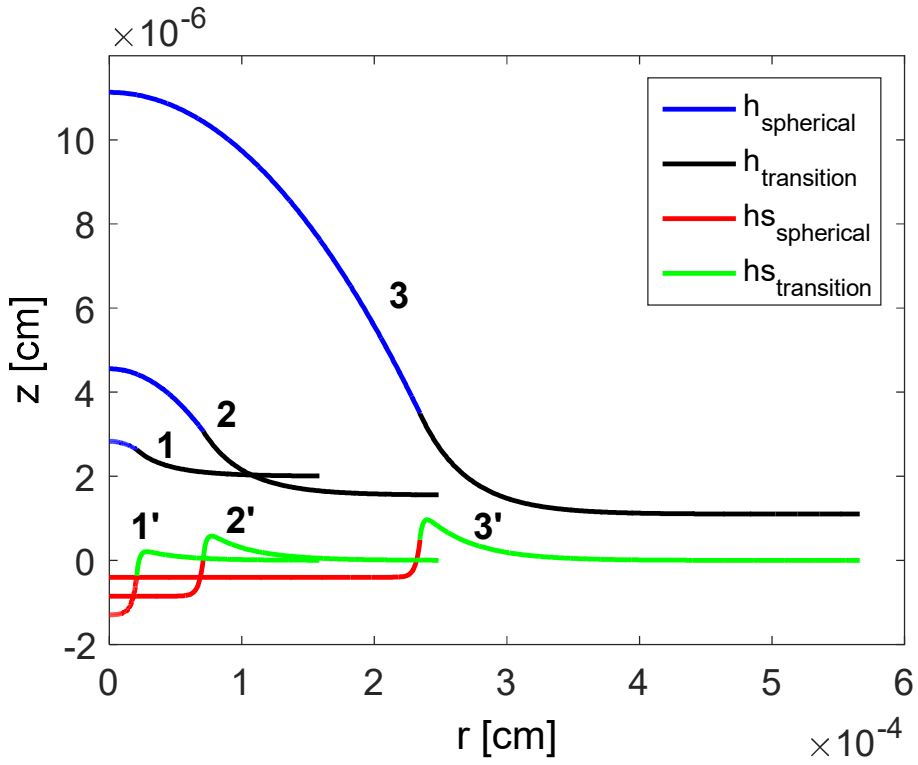

Figure 3: Calculated profiles of the droplet and substrate deformation: 1, 1′ − $|P_e| = 130000$ dyne/cm², 2, 2′ − $|P_e| = 85000$ dyne/cm², 3, 3′ − $|P_e| = 40000$ dyne/cm² [14]. . Reproduced with permission from Ref. [14]. Copyright © 2017 Elsevier B.V.

2.2. Effect of variation of slope of the disjoining/conjoining pressure isotherm, a

The value of a is varied in the following range $1 \times 10^{11} \leq a \leq 1 \times 10^{12}$ dyne/cm³ to see its impact on depth to which the substrate gets deformed and profile of the fluid droplet. Figure 4 demonstrates that slope a also effects the droplet shape: increasing the gradient of the disjoining/conjoining pressure isotherm, the maximum height of the droplet increases which correspondingly increases the effective radius of the droplet. The equilibrium contact angle for droplet on a deformable substrate increases as a increases. Slope of the adopted disjoining/conjoining pressure isotherm does not affect the extent/height to which the soft substrate gets deformed.

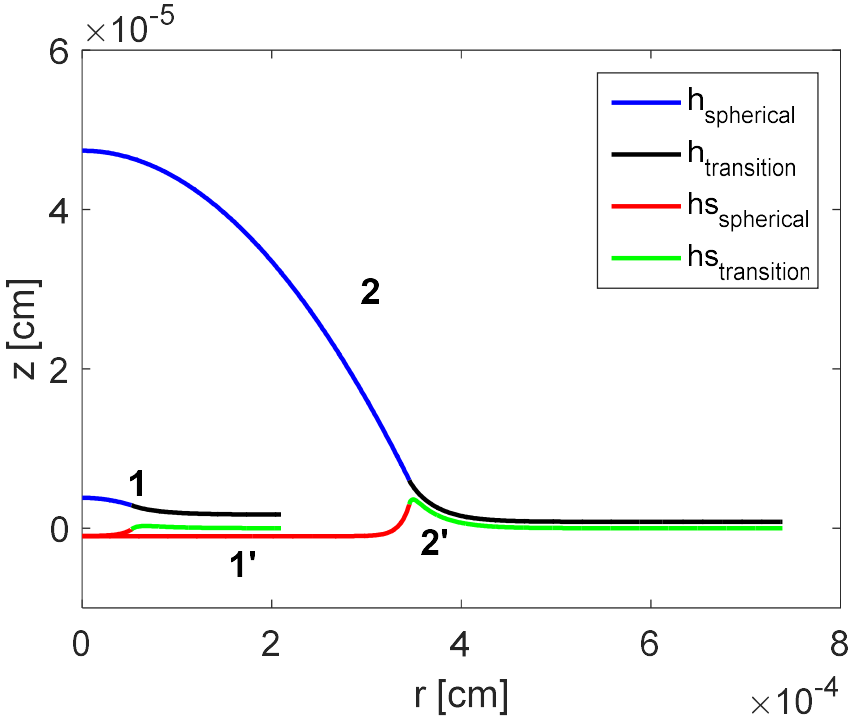

Figure 4: Calculated profiles of the droplet and substrate deformation: $1, 1' -$ $a = 1 \times 10^{11}$ dyne/cm^3, 2, $2' -$ $a = 1 \times 10^{12}$ dyne/cm^3 [14]. Reproduced with permission from Ref. [14]. Copyright © 2017 Elsevier B.V.

2.3. Effect of variation of elasticity coefficient, K

Elasticity coefficient controls the depth of deformation of the soft substrate. Here elasticity coefficient is changed according to $1 \times 10^{-13} \leq K \leq 1 \times 10^{-11}$ cm^3/dyne. The effect of decreasing the elasticity coefficient (i.e. $K \sim 0$) causes the outline of the droplet to approach the profile for non-deformable substrate which is apparent from Figure 5. It also shows that as K is increased (i.e. for a more elastic substrate) the equilibrium contact angle reduces marginally and the extent to which the soft substrate gets deformed increases (i.e. more deformation).

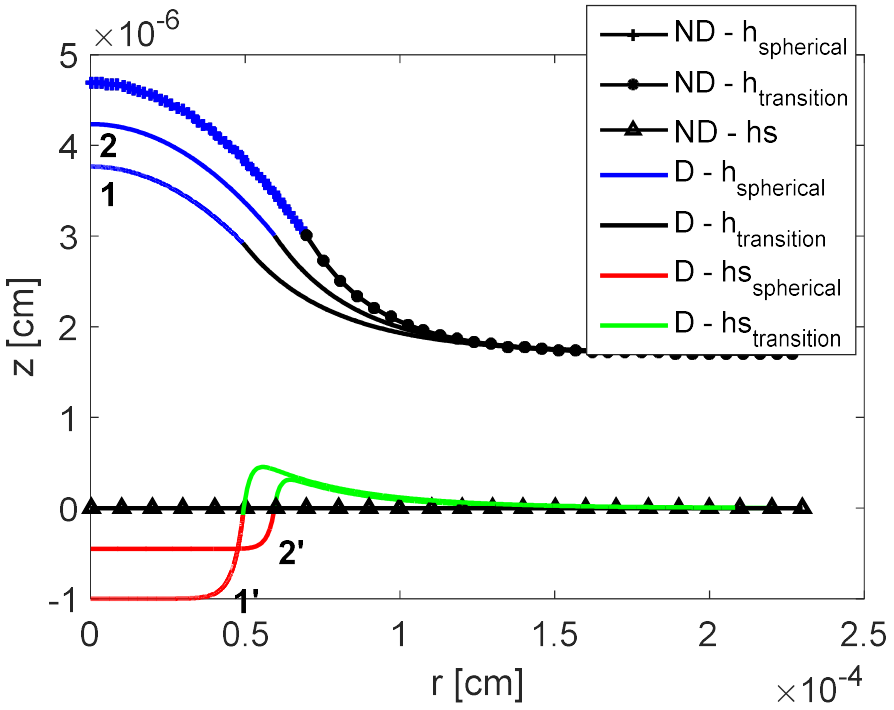

Figure 5: Calculated profiles of the droplet and substrate deformation: $1, 1' -$ $K = 1 \times 10^{-1}$ cm³/dyne, $2, 2' -$ $K = 4.5 \times 10^{-12}$ cm³/dyne, where "ND" stands for Non-Deformable substrate and "D" stands for Deformable substrate [14]. Reproduced with permission from Ref. [14]. Copyright © 2017 Elsevier B.V.

2.4. Effect of variation of substrate surface tension, γ_s

Substrate surface tension is varied according to $0.001 \leq \gamma_s \leq 30$ dyne/cm. Increasing γ_s causes equilibrium contact angle to increase a little as displayed in Figure 6. It also shows that there is a smooth transition of the substrate deformation from the bulk droplet to the region of thin films. However, when γ_s tends to zero this smooth transition in the substrate deformation tends to transform into a sharp jump.

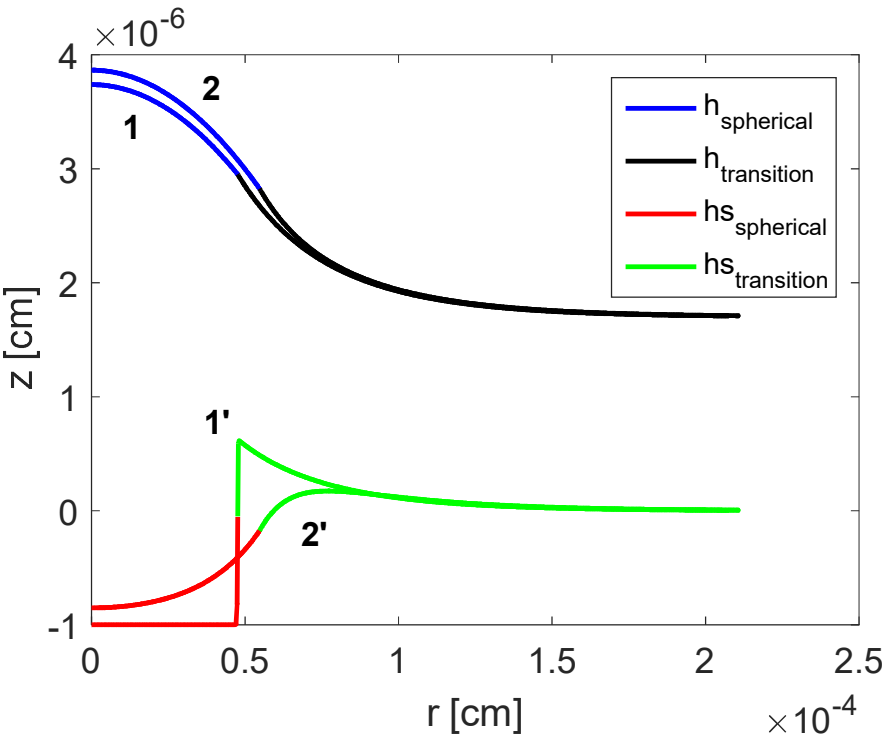

Figure 6: Calculated profiles of the droplet and substrate deformation: $1, 1' - \gamma_s = 0.001$ dyne/cm, $2, 2' - \gamma_s = 30$ dyne/cm [14]. Reproduced with permission from Ref. [14]. Copyright © 2017 Elsevier B.V.

3. Equilibrium conditions of droplets on deformable substrates

As stated in the previous section, excess free energy should be at its minimum value under equilibrium conditions. Solely in this situation, the obtained shapes of the liquid droplet and deformed substrate correspond to equilibrium. For the equilibrium, the following four essential conditions should be satisfied [11,16]:

1. The first variation of the free energy should be zero;
2. The second variation should be positive;
3. The transversality condition at the drop perimeter near the three-phase contact line should be satisfied [11];
4. Jacobi's sufficient condition should be satisfied. In the case of one-dimensional problem (a droplet on a rigid substrate), the solution of Jacobi's equation should not vanish at any position inside the area of investigation [11]. In the case of deformable substrate, the Jacobi's condition is specified below [16].

   Note, that conditions 1,2 and 3 are necessary conditions of the minimum of the excess free energy, while condition 4 is sufficient condition of the minimum. Altogether conditions 1,2,3,4 give necessary and sufficient conditions of the minimum of the excess free energy.

Unfortunately, the vital fourth condition of equilibrium is always neglected at consideration of deformation of soft solids under liquid droplets. Simply if the Jacobi's sufficient condition is fulfilled, the estimated profiles of the droplet and deformable substrate provide the minimum of free energy under equilibrium. For the first time, it was shown that the obtained solution truly (i.e. the fourth condition is satisfied) results in equilibrium profiles for the droplet and the deformable substrate [16].

Two-dimensional droplet is considered below for simplification and because Jacobi's condition is considerably easier to check in this case [16]. The excess free energy of a liquid droplet resting on a

deformable substrate is similar to the three-dimensional case discussed earlier with dimensional modifications in Eqs. (6) and (7), see Ref [16],

$$F_{2D} - F_{2De,film} = \int_0^\infty f_{2D}(h, h', h_s, h_s')dx, \tag{11}$$

where subscript 2D is for two-dimensional and

$$f_{2D}(h, h', h_s, h_s') = \begin{bmatrix} \gamma\sqrt{1 + h'^2(x)} - \gamma + \gamma_s\sqrt{1 + h_s'^2(x)} - \gamma_s + \\ P_e(h - h_s) - P_e h_e + \frac{h_s^2}{2K} - \frac{h_{se}^2}{2K} \\ + \int_{h-h_s}^\infty \Pi(h)dh - \int_{h_e}^\infty \Pi(h)dh \end{bmatrix}, \tag{12}$$

where x is the tangential co-ordinate. The corresponding equations for the two-dimensional droplet profile and deformed substrate are similar to the ones obtained for the three-dimensional case, i.e. Eqs. (8) and (9). Eqs. (8) and (9) in two-dimensional case are simplified to:

$$\frac{\gamma h''}{(1 + h'^2)^{3/2}} + \Pi(h - h_s) = P_e, \tag{13}$$

$$\frac{\gamma h_s''}{(1 + h_s'^2)^{3/2}} - \Pi(h - h_s) - \frac{h_s}{K} = -P_e, \tag{14}$$

Solution of Eqs. (13) and (14) using the physical properties mentioned in Table 1 is obtained in low slope approximation as above. Dependencies of both L_1 and apparent equilibrium contact angle, θ_e, are plotted against elasticity coefficient, K, shown in

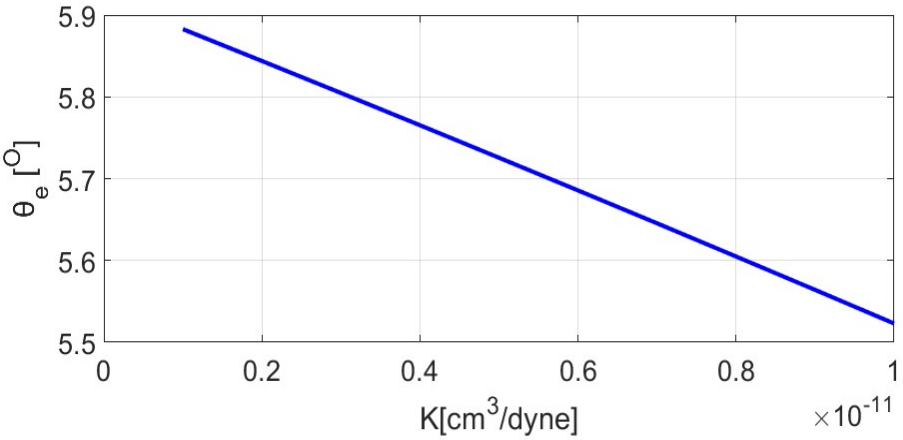

Figure 7: Equilibrium contact angle, θ_e, vs elasticity coefficient, K. Reproduced with permission from Ref. [16]. Copyright © 2018 Langmuir.

As expected, equilibrium contact angle decreases with the rise in the elasticity of the deformable substrate. Second necessary condition for the existence of a minimum of the excess free energy for the deformable substrate, $\delta^2 f_{2D} > 0$, is always satisfied [14]. Next is to check if Jacobi's sufficient condition is fulfilled.

To have Jacobi's condition of minimum to be achieved [12,16] the following should be satisfied: determinant built up by solutions of Jacobi's equation should not vanish at any position, x, inside the region of interest (see below). Under low slope approximation Jacobi equations for the four unknown functions $u_{ji}(x)$ are generated, where $i, j = 1, 2$ for the system of equations (11) and (12) are as follows:

$$\gamma u_{1i}'' + [\Pi'(h-h_s)u_{1i} - \Pi'(h-h_s)u_{2i}] = 0 \quad (15)$$

$$\gamma_s u_{2i}'' + \left[\Pi'(h-h_s)u_{1i} - \Pi'(h-h_s)u_{2i} + \frac{u_{2i}}{K}\right] = 0 \quad (16)$$

For a simplified disjoining/conjoining pressure isotherm (see Figure 2), Eqs. (15) and (16) become linear differential equations corresponding to all Jacobi's functions. Initial conditions for four Jacobi's functions [16,32]:

$$\left\{\begin{array}{c} u_{11}(0) = u_{12}(0) = u_{21}(0) = u_{22}(0) = 0 \\ u_{11}'(0) = 1\,,\; u_{22}'(0) = 1 \\ u_{12}'(0) = u_{21}'(0) = 0 \end{array}\right\} \quad (17)$$

Zero initial conditions and linearity of Jacobi's equations means that $u_{12}(x)$ and $u_{21}(x)$ are equal to zero. Therefore, there are only two unknowns, i.e., $u_{11}(x)$ and $u_{22}(x)$. Jacobi's condition, $D(x) = \begin{vmatrix} u_{11} & 0 \\ 0 & u_{22} \end{vmatrix} = u_{11}u_{22}$ should be positive for $x > 0$. According to Ref. [16], both $u_{11}(z)$ and $u_{22}(z)$ are positive for both spherical and transition regions, see Figure 2. This implies that D is positive at all $x > 0$ (see Figure 8). Jacobi's condition is therefore satisfied which means that solutions for both liquid and deformable substrate provide minimum of the excess free energy of the system [16].

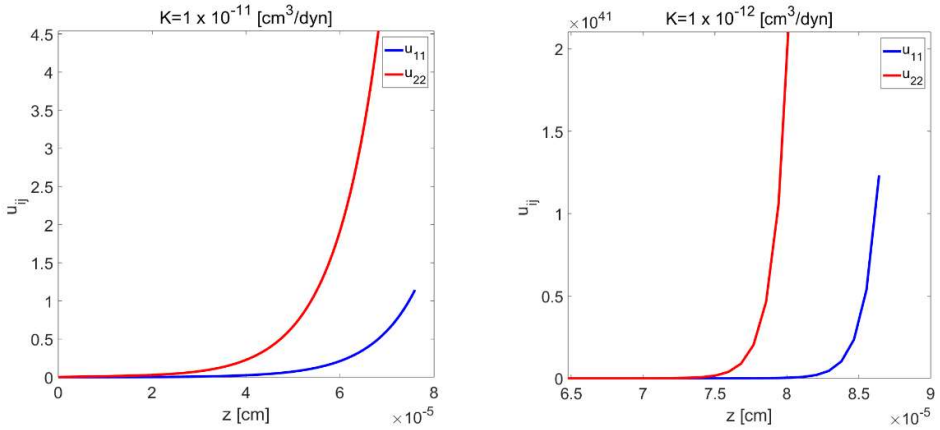

(**a**) (**b**)

Figure 8: Jacobi's functions $u_{11}(z)$ and $u_{22}(z)$ plotted against the length of the transition region $z(cm)$, for different elasticity coefficients. Reproduced with permission from Ref. [16]. Copyright © 2018 Langmuir.

Note, that the validity of the Jacobi's condition for the deduced solutions of both droplet shape and profile of the deformable substrate undertaken in [16], was checked for the first time. The latter means that any solution of the same problem developed earlier or to be developed in the future should be checked for a validity of the Jacobi's condition for the deduced solution.

4. Hysteresis of Contact Angle of Sessile Droplets on Deformable Substrates

Apparently, there is only a single equilibrium contact angle, θ_e, on smooth homogeneous substrates. However, according to Kelvin's equation to reach this equilibrium contact angle the droplet should be at the equilibrium with oversaturated vapor [11]. Therefore, experimentally only quasi equilibrium contact angles can be observed, which are referred to as hysteresis contact angles: static advancing contact angle $\theta_a > \theta_e$, and static receding contact angle $\theta_r < \theta_e$ [17].

Static advancing and receding contact angles are calculated in this using quasi-equilibrium states of a droplet on a soft substrate. Let us note, that such consideration was undertaken in [17] for the

first time and has never been tried before. Motion of the droplet starts when excess pressure is not equivalent to its value at equilibrium, $P \neq P_e$. This motion can be subdivided into "slow microscopic" before some critical values of applied pressure is reached and "fast macroscopic" processes above the critic value [17]. Fast macroscopic processes occur in the bulk/spherical part of the droplet whereas slow microscopic motion takes place in the transitional region (see Figure 9).

In advancing and receding droplets, transition from microscopic to macroscopic motion occurs when excess pressure approach critical values of P_a and P_r, respectively, with macroscopic contact angle reaching θ_a and θ_r, correspondingly. In advancing droplets, pressure is less than P_e, the slope of the profile grows and tends to infinity at some critical point (marked in Figure 9A) when P_a is reached. Apex, H_a, and the radius, R_a, of the advancing droplet are shown in Figure 9. When pressure is more than P_e, microscopically the slope of the droplet profile decreases causing it to become flat, i.e., zero slope, shown in Figure 9B. Where, H_r, is the apex and R_r, is the radius for a receding droplet (see Figure 9B). It was shown in [17] that quasi-equilibrium states of the droplet can be described using Eqs. (13) and (14) where the equilibrium pressure, P_e, is replaced by quasi-equilibrium pressures, P_a or P_r.

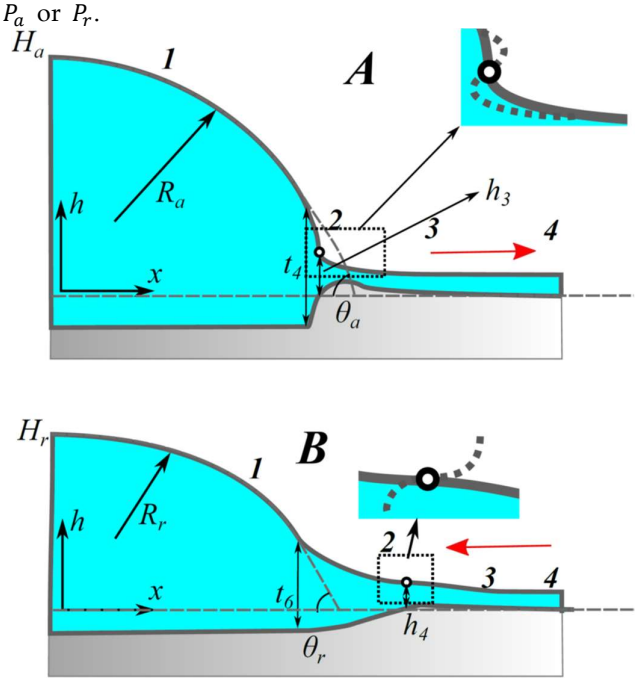

Figure 9: Droplet on a deformable substrate just before advancing (A) and just before receding (B) begins. 1- quasi-equilibrium part of the droplet; 2- inflection points; 3- flow zone; 4- equilibrium thin liquid film in front. Reproduced with permission from Ref. [17]. Copyright © 2018 Elsevier B.V.

Dangerous points (inflection points) exist in advancing and receding droplets. In advancing droplet inflection point is present at thickness, h_3, and in receding droplet inflection point is present at thickness, h_4 [17,30] (see Figure 9). Boundary conditions for both cases are:

$$h'' = 0, \quad h' = -\infty, \quad at \ h = h_3. \tag{18}$$

$$h'' = 0, \quad h' = 0, \quad at \ h = h_4. \tag{19}$$

Numerical solution is only possible for Eqs. (13) and (14), because of their coupled nature. To simplify calculations, piecewise linear function of h disjoining/conjoining pressure isotherm is adopted [17]:

Peer-reviewed version available at Colloids Interfaces 2018, 2, 56; doi:10.3390/colloids2040056

$$\Pi(h) = \begin{cases} a(t_0 - h) & 0 \le h \le t_1 \\ b(h - t_2) & t_1 \le h \le t_3 \\ c(t_4 - h) & t_3 \le h \le t_5 \\ d(h - t_6) & t_5 \le h \le t_6 \\ 0 & h > t_6 \end{cases}, \quad (20)$$

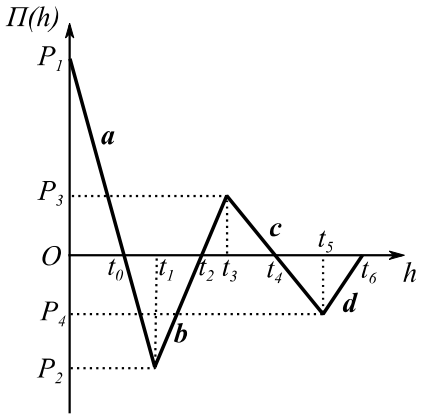

Figure 10: Piece-wise linear disjoining/conjoining pressure isotherm for quasi-equilibrium cases. Reproduced with permission from Ref. [17]. Copyright © 2018 Elsevier B.V.

where $t_1, t_2, t_3, t_4, t_5, t_6$ are different regions of adopted disjoining/conjoining pressure isotherm, and a, b, c, d are corresponding slopes of these regions. Adopted disjoining/conjoining pressure isotherm has following vital properties: (i) stability condition, $\Pi'(h) < 0$ when $0 \le h \le t_1$ (α-films [11] and $t_3 < h < t_5$ (β-films [11]) is satisfied; (ii) corresponds to partial wetting; (iii) surface forces action is short ranged, i.e. $h = t_6$. These parameters are carefully selected to resemble as closely as possible the actual disjoining/conjoining pressure isotherm used in Ref. [30] in order to verify calculations of advancing/receding contact angles on solid/rigid substrates, see Table 2 and Figure 10 [17]. The additional simplification adopted in [17] is as follows γ_s , that is solid/liquid interfacial tension has been neglected. However, in this case the low slope approximation has not been used.

Table 2: Properties of disjoining/conjoining pressure isotherm for advancing/receding contact angles [17].

Physical Properties	Values
γ	72.00 dyne/cm
P_1	1.300×10^{13} dyne/cm^2
P_2	-4.450×10^{8} dyne/cm^2
P_3	2.800×10^{7} dyne/cm^2
P_4	-6.500×10^{4} dyne/cm^2
t_0	$\frac{P_1}{a} = 2.299 \times 10^{-8}$ cm
t_1	2.300×10^{-8} cm
t_2	$t_3 - \frac{P_3}{b} = 2.083 \times 10^{-7}$ cm
t_3	2.200×10^{-7} cm
t_4	3.000×10^{-6} cm
t_5	3.007×10^{-6} cm
t_6	2.000×10^{-5} cm
a	$\frac{P_1 - P_2}{t_1} = 5.652 \times 10^{20}$ dyne/cm^3

b	$\frac{P_3-P_2}{t_3-t_1} = 2.401 \times 10^{15}$ dyne/cm^3
c	$\frac{P_3}{t_4-t_3} = 1.007 \times 10^{13}$ dyne/cm^3
d	$\frac{P_4}{t_5-t_6} = 3.825 \times 10^{9}$ dyne/cm^3
K	2.000×10^{-16} cm^3/dyne, i.e., $bK < 1$
V_a	1.000×10^{-2} cm^2

Effect of variation of volume of the advancing droplet on advancing contact θ_a was investigated, see Figure 11a. As the volume of the droplet increases the advancing contact angle reduces. Advancing contact angle on a deformable substrate is always less than on a non-deformable substrate [17,30]. Figure 11b shows the effect of variation of volume on receding contact angle. As the volume of the droplet increases the receding contact angle reduces. Elasticity of the deformable substrate causes a decrease in receding contact angle in comparison with solid substrate, but the extent of decrease is very small as seen from Figure 11b. Advancing, and receding contact angles decrease for a soft substrate. This behavior has been experimentally observed [33,34].

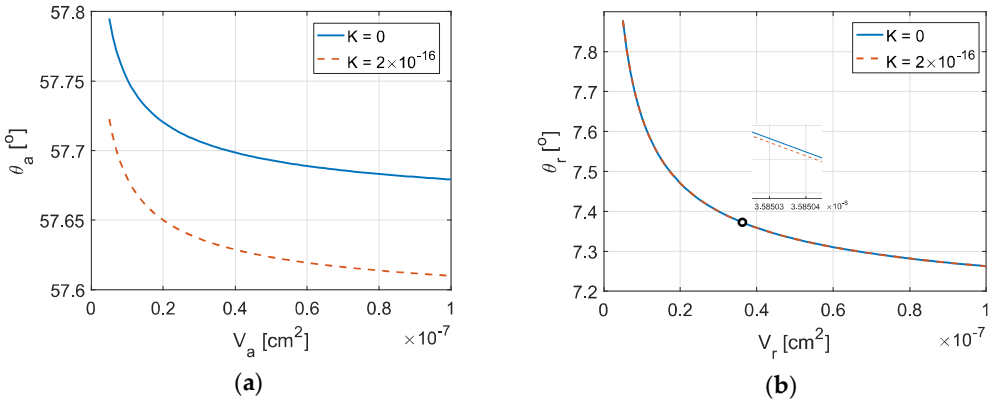

Figure 11: Effect of variation of volume of the droplet on (a) advancing and (b) receding contact angles. Reproduced with permission from Ref. [17]. Copyright © 2018 Elsevier B.V.

Funding: This research was funded by CoWet project from EU, MAP EVAPORATION project from European Space Agency and Proctor & Gamble, Brussels.

Acknowledgments: This research was supported by CoWet Marie Curie EU project; and MAP EVAPORATION project, European Space Agency and Proctor & Gamble, Brussels.

Nomenclature

a, b, c, d	–	Slopes of different regions of disjoining/conjoining pressure isotherm
α	–	α –film
β	–	β –film
D	–	Deformable substrate
$D(x)$	–	Jacobi condition
F, F_{2D}	–	Excess free energy in three and two-dimensional cases
$F_{e,film}$, $F_{2De,film}$	–	Excess free energy of the equilibrium thin film on the deformed solid in three and two-dimensional cases
γ	–	Surface tension of the fluid
γ_s	–	Surface tension of the substrate
H	–	Apex of the droplet
H_a	–	Apex of the advancing droplet

Peer-reviewed version available at Colloids Interfaces 2018, 2, 56; doi:10.3390/colloids2040056

H_r	–	Apex of the receding droplet
h	–	Film thickness, equilibrium liquid profile, droplet height
h_e	–	Stable equilibrium film thickness
h_s	–	Local deformation of the substrate
h_{se}	–	Local deformation of the substrate under the action of the ambient pressure
h_3	–	Thickness in the critical point for advancing droplet
h_4	–	Thickness in the critical point for receding droplet
K	–	Elasticity coefficient
l	–	Characteristic length
μ	–	Dynamic viscosity
ND	–	Non-deformable substrate
P_{air}	–	Pressure in the ambient air
P_e	–	Equilibrium excess pressure
P_a	–	Advancing pressure
P_r	–	Receding pressure
p	–	Vapor pressure
p_{sat}	–	Saturated vapor pressure
$\Pi(h)$	–	Disjoining/conjoining pressure isotherm
Q	–	Flow rate
R	–	Radius of curvature of the droplet
R_a	–	Radius of curvature of the advancing droplet
R_g	–	Gas constant
R_r	–	Radius of curvature of the receding droplet
r	–	Length along radial direction for three-dimensional case
T	–	Temperature
$t_0, t_1, t_2, t_3, t_4, t_5, t_6$	–	Parameters of disjoining/conjoining pressure isotherm
θ_e	–	Equilibrium contact angle
θ_a	–	Advancing contact angle
θ_r	–	Receding contact angle
$u(x)$	–	Solution of Jacobi's equation
V	–	Volume of the fluid
V_a	–	Volume of the advancing droplet
V_r	–	Volume of the receding droplet
v_m	–	Molar volume of the liquid
x	–	Length along radial direction for two-dimensional case
$z = x - L_1$	–	Co-ordinate in the tangential direction

References

1. Bonn, D.; Eggers, J.; Indekeu, J.; Meunier, J. Wetting and spreading. *Rev. Mod. Phys.* **2009**, *81*, 739–805, doi:10.1103/RevModPhys.81.739.
2. Attinger, D.; Moore, C.; Donaldson, A.; Jafari, A.; Stone, H. A. Fluid dynamics topics in bloodstain pattern analysis: Comparative review and research opportunities. *Forensic Sci. Int.* **2013**, *231*, 375–396, doi:10.1016/j.forsciint.2013.04.018.
3. Eral, H. B.; 'T Mannetje, D. J. C. M.; Oh, J. M. Contact angle hysteresis: A review of fundamentals and applications. *Colloid Polym. Sci.* **2013**, *291*, 247–260, doi:10.1007/s00396-012-2796-6.
4. Young, T. An Essay on the Cohesion of Fluids. *Philos. Trans. R. Soc. London* **1805**, *95*, 65–87, doi:10.1098/rstl.1805.0005.
5. Lester, G. . Contact angles of liquids at deformable solid surfaces. *J. Colloid Sci.* **1961**, *16*, 315–326, doi:10.1016/0095-8522(61)90032-0.
6. Rusanov, A. Theory of wetting of elastically deformed bodies. 1. Deformation with a finite contact-angle. *Colloid J.* **1975**, *37*, 614–622.
7. Rusanov, A. Theory of wetting of elastically deformed bodies. 2. Equilibrium conditions and work of deformation with a finite contact angle. *Colloid J.* **1975**, *37*, 623–628.
8. Rusanov, A. On the thermodynamics of deformable solid-surfaces. *J. Colloid Interface Sci.* **1978**, *63*, 330–345, doi:10.1016/0021-9797(78)90142-X.
9. Shanahan, M. E. R. The Spreading Dynamics of a Liquid-Drop on a Viscoelastic Solid. *J. Phys. D-Applied Phys.* **1988**, *21*, 981–985, doi:10.1088/0022-3727/21/6/019.
10. Shanahan, M.; de gennes, P. The ridge produced by a liquid near the triple line solid liquid fluid. *Comptes Rendus L Acad. Des Sci. Ser. II* **1986**, *302*, 517–521.
11. Starov, V. M.; Velarde, M. G.; Radke, C. J. *Wetting and Spreading Dynamics*; CRC Press Taylor and Francis Group, 2007;
12. Derjaguin, B. V.; Churaev, N. V.; Muller, V. M. *Surface Forces*; Springer US, 1987;
13. White, L. R. The contact angle on an elastic substrate. 1. The role of disjoining pressure in the surface mechanics. *J. Colloid Interface Sci.* **2003**, *258*, 82–96, doi:10.1016/S0021-9797(02)00090-5.
14. Ahmed, G.; Kalinin, V. V; Arjmandi-tash, O.; Starov, V. M. Equilibrium of droplets on a deformable substrate: Influence of disjoining pressure. *Colloids Surfaces A Physicochem. Eng. Asp.* **2017**, *521*, 3–12, doi:10.1016/j.colsurfa.2016.06.057.
15. Arjmandi-Tash, O.; Kovalchuk, N. M.; Trybala, A.; Kuchin, I. V.; Starov, V. Kinetics of Wetting and Spreading of Droplets over Various Substrates. *Langmuir* **2017**, *33*, 4367–4385, doi:10.1021/acs.langmuir.6b04094.
16. Koursari, N.; Ahmed, G.; Starov, V. M. Equilibrium Droplets on Deformable Substrates: Equilibrium Conditions. *Langmuir* **2018**, *34*, 5672–5677, doi:10.1021/acs.langmuir.8b00635.
17. Ahmed, G.; Koursari, N.; Kuchin, I. V; Starov, V. M. Hysteresis of Contact Angle of Sessile Droplets on Deformable Substrates : In fl uence of Disjoining Pressure. *Colloids Surfaces A* **2018**, *546*, 129–135, doi:10.1016/j.colsurfa.2018.03.006.
18. Carre, A.; Shanahan, M. E. R. Viscoelastic Braking of a Running Drop. *Langmuir* **2001**, 2982–2985, doi:10.1021/la001600e.
19. Jerison, E. R.; Xu, Y.; Wilen, L. A.; Dufresne, E. R. Deformation of an Elastic Substrate by a Three-Phase Contact Line. *Phys. Rev. Lett.* **2011**, *106*, 186103, doi:10.1103/PhysRevLett.106.186103.
20. Park, S. J.; Weon, B. M.; Lee, J. S.; Lee, J.; Kim, J.; Je, J. H. Visualization of asymmetric wetting ridges on soft solids with X-ray microscopy. *Nat. Commun.* **2014**, *5*, 4369, doi:10.1038/ncomms5369.
21. Schulman, R. D.; Dalnoki-Veress, K. Liquid Droplets on a Highly Deformable Membrane. *Phys. Rev. Lett.* **2015**, *115*, 206101, doi:10.1103/PhysRevLett.115.206101.
22. Style, R. W.; Boltyanskiy, R.; Che, Y.; Wettlaufer, J. S.; Wilen, L. A.; Dufresne, E. R. Universal Deformation of Soft Substrates Near a Contact Line and the Direct Measurement of Solid Surface Stresses. *Phys. Rev. Lett.* **2013**, *110*, 066103, doi:10.1103/PhysRevLett.110.066103.
23. Lubbers, L. A.; Weijs, J. H.; Botto, L.; Das, S.; Andreotti, B.; Snoeijer, J. H. Drops on soft solids: free energy and double transition of contact angles. *J. Fluid Mech.* **2014**, *747*, R1, doi:10.1017/jfm.2014.152.
24. Limat, L. Straight contact lines on a soft, incompressible solid. *Eur. Phys. J. E* **2012**, *35*, 134, doi:10.1140/epje/i2012-12134-6.

25. Marchand, A.; Das, S.; Snoeijer, J. H.; Andreotti, B. Contact Angles on a Soft Solid: From Young's Law to Neumann's Law. *Phys. Rev. Lett.* **2012**, *109*, 236101, doi:10.1103/PhysRevLett.109.236101.
26. Bico, J.; Reyssat, É.; Roman, B. Elastocapillarity: When Surface Tension Deforms Elastic Solids. *Annu. Rev. Fluid Mech.* **2018**, doi:10.1146/annurev-fluid-122316-050130.
27. Winkler, E. The theory of elasticity and strength with special reference to their application in the art for polytechnics, building academies, engineers, mechanical engineers, Architects, Etc. In *H. Dominicus*; 1867.
28. Starov, V. Static contact angle hysteresis on smooth, homogeneous solid substrates. *Colloid Polym. Sci.* **2013**, *291*, 261–270.
29. Kuchin, I.; Starov, V. Hysteresis of the Contact Angle of a Meniscus Inside a Capillary with Smooth, Homogeneous Solid Walls. *Langmuir* **2016**, *32*, 5333–5340, doi:10.1021/acs.langmuir.6b00721.
30. Kuchin, I.; Starov, V. Hysteresis of Contact Angle of Sessile Droplets on Smooth Homogeneous Solid Substrates via Disjoining/Conjoining Pressure. *Langmuir* **2015**, *31*, 5345–5352, doi:10.1021/acs.langmuir.5b01075.
31. Kerr, A. D. Elastic and Viscoelastic Foundation Models. *J. Appl. Mech.* **1964**, *31*, 491–498, doi:10.1115/1.3629667.
32. Gelfand, I. M.; Fomin, S. V. *Calculus of Variations*; Prentice-Hall, Inc.: Englewood Cliffs, N.J., 1963;
33. Bormashenko, E.; Bormashenko, Y.; Whyman, G.; Pogreb, R.; Musin, A.; Jager, R.; Barkay, Z.; Uni, A.; Applied, W. Contact Angle Hysteresis on Polymer Substrates Established with Various Experimental Techniques, Its Interpretation, and Quantitative Characterization. *Langmuir* **2008**, *8*, 4020–4025, doi:10.1021/la703875b.
34. Rioboo, R.; Voué, M.; Adão, H.; Conti, J.; Vaillant, A.; Seveno, D.; De Coninck, J. Drop impact on soft surfaces: Beyond the static contact angles. *Langmuir* **2010**, *26*, 4873–4879, doi:10.1021/la9036953.